Current Optics and Photonics
Vol. 2, No. 3, June 2018, pp. 269-279

ISSN: 2508-7266(Print) / ISSN: 2508-7274(Online)
DOI: https://doi.org/10.3807/COPP.2018.2.3.269

Performance Prediction of a Laser-guide Star Adaptive Optics System for a 1.6 m Telescope

Jun Ho Lee[1]*, Sang Eun Lee[2], and Young Jun Kong[2]

[1]Department of Optical Engineering, Kongju National University, Cheonan 31080, Korea
[2]Electro-Optics Research Center, LigNex1, Yongin 16911, Korea

(Received May 10, 2018 : revised May 24, 2018 : accepted May 24, 2018)

We are currently investigating the feasibility of a 1.6 m telescope with a laser-guide star adaptive optics (AO) system. The telescope, if successfully commissioned, would be the first dedicated adaptive optics observatory in South Korea. The 1.6 m telescope is an *f*/13.6 Cassegrain telescope with a focal length of 21.7 m. This paper first reviews atmospheric seeing conditions measured over a year in 2014~2015 at the Bohyun Observatory, South Korea, which corresponds to an area from 11.6 to 21.6 cm within 95% probability with regard to the Fried parameter of 880 nm at a telescope pupil plane. We then derive principal seeing conditions such as the Fried parameter and Greenwood frequency for eight astronomical spectral bands (V/R/I/J/H/K/L/M centered at 0.55, 0.64, 0.79, 1.22, 1.65, 2.20, 3.55, and 4.77 μm). Then we propose an AO system with a laser guide star for the 1.6 m telescope based on the seeing conditions. The proposed AO system consists of a fast tip/tilt secondary mirror, a 17 × 17 deformable mirror, a 16 × 16 Shack-Hartmann sensor, and a sodium laser guide star (589.2 nm). The high order AO system is close-looped with 2 KHz sampling frequency while the tip/tilt mirror is independently close-looped with 63 Hz sampling frequency. The AO system has three operational concepts: 1) bright target observation with its own wavefront sensing, 2) less bright star observation with wavefront sensing from another bright natural guide star (NGS), and 3) faint target observation with tip/tilt sensing from a bright natural guide star and wavefront sensing from a laser guide star. We name these three concepts '*None*', '*NGS only*', and '*LGS + NGS*', respectively. Following a thorough investigation into the error sources of the AO system, we predict the root mean square (RMS) wavefront error of the system and its corresponding Strehl ratio over nine analysis cases over the worst (2σ) seeing conditions. From the analysis, we expect Strehl ratio >0.3 in most seeing conditions with guide stars.

Keywords : Adaptive optics, Atmospheric turbulence, Telescope, Strehl ratio
OCIS codes : (220.1080) Active or adaptive optics; (080.2740) Geometric optical design; (010.1330) Atmospheric turbulence; (120.4640) Optical instruments

I. INTRODUCTION

Optical images of astronomical objects such as stars produced by ground telescopes are blurred, moving, or scintillating due to Earth's atmosphere [1]. This is due to the optical refractive index variations caused by atmospheric turbulent mixing. The atmospheric disturbance limits the achievable angular resolution of ground telescopes regardless of the aperture size, and this is commonly known as seeing or astronomical seeing at a particular site. For even excellent sites under the best seeing conditions, large-aperture telescopes are not able to resolve objects any better than those with an aperture of ~20 cm, even though they efficiently collect light.

An adaptive optics (AO) system is typically an auxiliary instrument to a ground telescope and it has shown great promise for improving astronomical seeing beyond the limits imposed by atmospheric turbulence [2]. AO systems

*Corresponding author: jhlsat@kongju.ac.kr, ORCID 0000-0002-4075-3504
Color versions of one or more of the figures in this paper are available online.

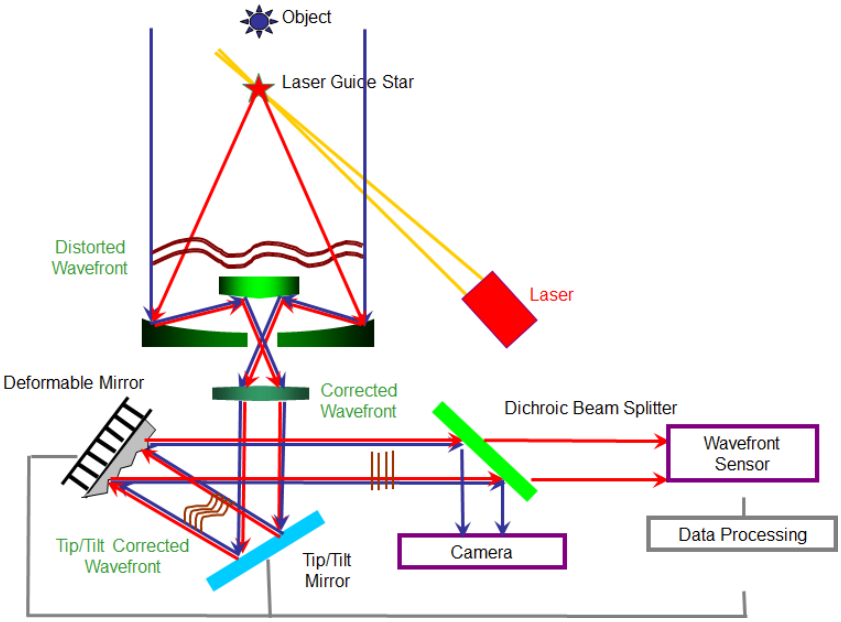

FIG. 1. Schematic diagram of a laser-guide star adaptive optics system.

compensate the wavefront distortion introduced by the atmosphere by introducing controllable counter wavefront distortion that both spatially and temporally follows that of the medium. A large ground telescope with an adaptive optics system typically consists of a telescope, relay optics, a tip/tilt mirror, a deformable mirror, a scientific camera, a wavefront sensor, a laser guide star, and a data processing or control system (Fig. 1). A laser guide star (LGS), also known as an artificial guide star, is required as a point reference source of light for measuring and correcting wavefront distortions when any bright stars, known as natural guide stars (NGSs), are not available within the isoplanatic angle, i.e. the angle at which the AO corrections are valid. A solution to create a laser guide star is the sodium-beacon approach, which is of interest in this paper [3-5]. This approach focuses laser light of the sodium D2 line (589 nm) to excite a layer of sodium atoms that are present in the mesosphere at an altitude of ~90 km, which then appear as a star. The laser guide star can serve as a wavefront reference in the same way as a natural guide star except that natural reference stars, which could be much fainter than NGSs, are still required for image position (tip/tilt) information.

We are currently investigating the feasibility of a 1.6 m telescope with a laser-guide star adaptive optics (AO) system. The telescope, if successfully commissioned, would be the first dedicated adaptive optics observatory in South Korea. The 1.6 m telescope is an *f*/13.6 Cassegrain telescope with a focal length of 21.7 m. The AO system consists of a tip/tilt secondary mirror, a deformable mirror, two scientific cameras (CCD and IR detector), a Shack-Hartman wavefront sensor, a laser guide star, and a data processing or control system (Fig. 1).

This paper first presents the system design of the AO system based on the seeing conditions measured at the Bohyun Observatory, South Korea, which is one of the telescope site candidates. We then investigate the imaging performance of the telescope in terms of the Strehl ratio predicted at four wave bands (V/I/J/K/L centered at 0.55, 0.79, 1.26, 2.22, and 3.4 μm) for NGS and LGS cases. The prediction considers a wide range of parameters and error sources, including the strength and profile of the atmospheric turbulence, the fitting error caused by the finite spatial resolutions of the wavefront sensor and deformable mirror, wavefront sensor noise propagating through the wavefront reconstruction algorithm, servo lag resulting from the finite bandwidth of the control loop, and the anisoplanatism for a given constellation of natural and/or laser guide stars [6-10].

II. BRIEF DESCRIPTION OF THE 1.6 m TELESCOPE

The telescope is an *f*/13.6 Nasmyth-Cassegrain telescope on an alt-azimuth mount, which is a simple two-axis mount for supporting and rotating an instrument about two perpendicular axes - one vertical and the other horizontal. As in the Cassegrain telescope, the light falls on a concave primary mirror and then is reflected toward a convex secondary mirror. A small 45° tilted tertiary flat mirror, placed on the altitude axis, focuses the light through a hole in the middle of the altitude bearing to one of the sides of the telescope called the Nasmyth focus. Table 1 lists the major specifications and Fig. 2 shows the optical layout and a 3D model of the telescope.

The telescope is equipped with a laser launch telescope

TABLE 1. Specifications of the 1.6 m telescope

Item	Values	Note
Type	Nasmyth-Cassegrain	
Entrance pupil diameter	1.6 m	Located at the primary mirror
Central obstruction	0.28	
F number	13.6	Paraxial
Focal length	21.7 m	
Exit pupil position	4387 mm	Distance before the image plane
Exit pupil diameter	336 mm	Re-imaged with a parabolic mirror on a deformable mirror of 24.5 mm diameter
Design field of view	0.07° (0.05° × 0.05°)	0.36° (0.3° × 0.2°) for a guide camera

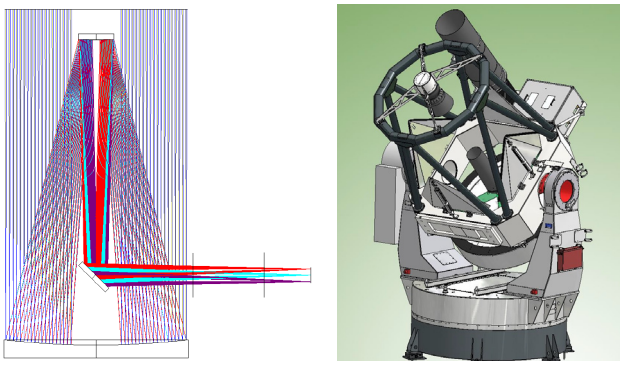

(a) (b)

FIG. 2. Optical layout and 3D model of the 1.6 m telescope. (a) Optical layout, (b) 3D model.

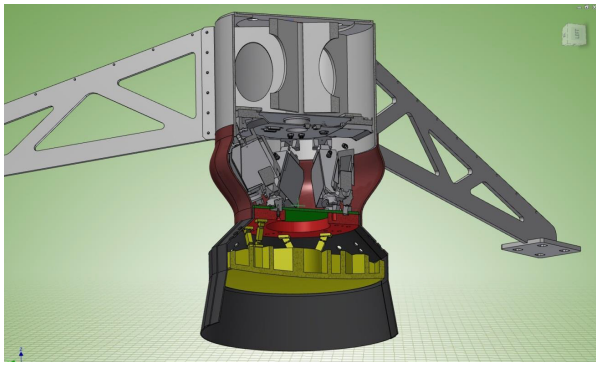

FIG. 3. Mechanical model of the adaptive secondary mirror mounted on a tip/tilt platform.

with a sodium laser, an AO system set, and two scientific cameras (a CCD and an IR detector). The laser launch telescope with the laser head is mounted on the center frame, the laser electric control box is mounted on one of the Nasmyth platforms, and the optical bench including the AO system is set on the other Nasmyth port. The secondary mirror is mounted on a tip/tilt platform so it works as a tip/tilt mirror and also as an IR chopping mirror for subtracting IR backgrounds from IR observations [11], as shown in Fig. 3.

III. ATMOSPHERIC CONDITIONS AT THE SITE

3.1. Background of Astronomical Seeing

The theoretical resolution limit of a telescope is given by Rayleigh criterion [12]:

$$\theta = 1.22\frac{\lambda}{D}, \tag{1}$$

where θ is the angular resolution, λ the wavelength of incoming light, and D the telescope aperture. A telescope's effective angular resolution is further limited by atmospheric disturbance. The limited resolution or quality of the optical imaging at a particular site is referred to as seeing or astronomical seeing, which is commonly described in two ways: (1) the full width at half maximum of a star's intensity distribution at the focus of a telescope in angle (θ_{seeing}), (2) the Fried parameter (r_o) representing the spatial size of a typical lump of uniform air within the turbulent atmosphere. The limited angular resolution or seeing θ_{seeing} is related to the Fried parameter (r_o) as follows [2]:

$$\theta_{seeing} = 0.98\frac{\lambda}{r_o}. \tag{2}$$

The Fried parameter (r_o) is then related to the spatial and temporal variation of the refractive index of the air that the beam comes through. The variation of the refractive index is typically measured by the refractive index structure parameter C_n^2, where the average C_n^2 is often determined as a function of local differences in the temperature, moisture, and wind velocity at discrete points. The Kolmogorov model of turbulence states that the Fried parameter (r_o) is a function of the index structure parameter and the wavelength, as given below [13].

$$r_0 = 0.185\lambda^{6/5}\cos^{3/5}\varsigma\left(\int C_n^2(h)dh\right)^{-3/5}. \tag{3}$$

Here, $C_n^2(h)$ is the refractive index structure parameter at altitude h, the observed wavelength is λ, and the observed

angle is ς. Roddier similarly defined the coherence time or critical time constant (τ_o) from the Fried parameter and the average velocity of the turbulence (V_o), which corresponds to the duration over which the standard deviation of the phase fluctuations at a given point is of the order of 1 rad [14, 15].

The Greenwood frequency (f_G) is then defined as the frequency or bandwidth required for optimal correction with an adaptive optics system [16]. The Greenwood frequency is a measure of how fast the AO system must respond. Typically, the closed-loop bandwidth of the AO system is practically taken to be about 1/10~1/12.5 of the wavefront sampling frequency. Analogous to the Greenwood frequency, a fundamental tracking frequency (f_T) is also defined as the frequency or bandwidth required for optimal tip/tilt correction [17].

$$V_o = \left(\frac{\int V(h)^{5/3} C_n^2(h) dh}{\int C_n^2(h) dh} \right)^{3/5}, \tag{4}$$

$$\tau_0 = 0.314 \frac{r_o}{V_o}, \tag{5}$$

$$f_G = 0.134 \frac{1}{\tau_0}, \tag{6}$$

$$f_T = 0.331 D^{-1/6} \lambda^{-1} \left[\sec(\varsigma) \int V(h)^2 C_n^2(h) dh \right]^{1/2} \approx 0.0811 \left(\frac{r_0}{D} \right)^{1/6} \left(\frac{V}{r_0} \right). \tag{7}$$

The time-averaged atmospheric disturbance is independent of the viewing direction because the turbulence and its structure function are statistically the same everywhere in the field. But the instantaneous atmospheric phase aberrations do depend on the viewing direction. Hence there is an angular limitation called the isoplanatic angle θ_0 within which effective AO corrections can still be made. The isoplanatic angle is defined as the angle for which the RMS (root-mean-squared) wavefront phase error has increased by 1 radian. Analogous to the isoplanatic angle, the isoplanatic tilt angle (θ_{TA}) for tip/tilt sensing can be similarly defined as follows [18];

$$\theta_o = \left(2.91 \left(\frac{2\pi}{\lambda} \right)^2 \sec^{8/3} \varsigma \int C_n^2(h) h^{5/3} dh \right)^{-3/5}, \tag{8}$$

$$\theta_{TA} = \left(0.668 \left(\frac{2\pi}{\lambda} \right)^2 D^{-1/3} \sec^3 \varsigma \int C_n^2(h) v(h)^2 dh \right)^{-1/2} \approx 4\theta_o. \tag{9}$$

The above equation is approximated by the following equation. H is a characteristic average turbulence altitude. The averaging is done by weighting the $C_n^2(h)$ profile with $h^{5/3}$; as a result a relatively high $H \sim 5$ km is obtained for typical conditions.

$$\theta_o = 0.31 \frac{r_0}{H}. \tag{10}$$

3.2. Seeing Measurement with SLODAR at the Site

One of the site candidates for the 1.6 m telescope is the Bohyun observatory located at 36.1648°N and 128.977°E with altitude 1124 m. Astronomical seeing was monitored at the site for a year starting in June of 2014 by a seeing monitor called SLODAR (SLOpe Detection And Ranging) [10, 19-21]. The SLODAR measured the vertical profile of $C_n^2(h)$ with the total seeing (r_o) at 500 nm. Since the SLODAR was remotely operated without on-site human presence, the SLODAR was cautiously operated only under specific weather conditions: no rain/snow and humidity under 70%. In addition, the measurement was further

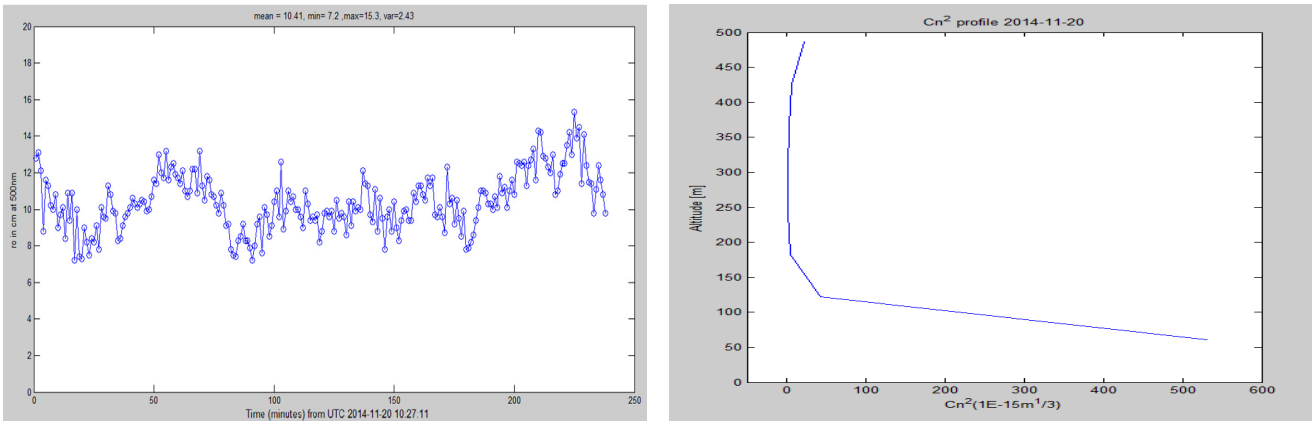

(a) (b)

FIG. 4. SLODAR results measured at 500 nm over 20 Nov. 2014. (a) Temporal variation of the total seeing (r_o) value, (b) Refractive index structure parameter at altitude h, $C_n^2(h)$.

hindered by cloud coverage since the SLODAR requires a binary star with a specific angular separation at the observation direction. As results, the seeing data were recorded over 23 nights in total for the one year campaign. Due to the small number of observation nights, it is premature to draw conclusions on the seeing conditions but it is still valid to present the baselines. Figure 4 shows the temporal variation of the total seeing (r_o) and refractive index structure parameter at altitude *h*, $C_n^2(h)$ measured at 500 nm over one night (20 Nov. 2014).

A weather station, located beside the SLODAR, continuously recorded environmental conditions including temperature, humidity, and ground wind speed over the year. The average ground speed was 2.58 m/sec with a standard deviation (sigma) of 0.89 m/sec and the instant maximum speed was 20.8 m/sec. However, the measurements were adequate for predicting the average velocity of the turbulence (V_o), which requires a wind profile up to ~15 km beyond a strong wind shear layer occurring near the tropopause at 8~12 km height [22]. García-Lorenzo *et al*. reported experimental prediction of the average velocity of the turbulence (V_o) from the mean ground velocity (V_{ground}) [23, 24] as follows, where the average velocity of the turbulence (V_o) at the site is estimated with two sigma values to be around 6.76~9.72 m/sec with a nominal value of 8.29 m/sec, which is in good accordance with measurements performed at other astronomical telescope sites.

$$V_o \approx 0.833\, V_{ground} + 6.09 \tag{11}$$

3.3. Statistical Prediction Seeing Conditions at the Site

Table 2 lists the statistical predictions of seeing conditions at some optical bands (V/R/I/J/H/K/L/M centered at 0.55, 0.64, 0.79, 1.22, 1.65, 2.20, 3.55, and 4.77 μm), which are derived from the SLODAR measurements at 0.5 μm over the 23 nights. The total seeing (r_{o,λ_1}) at one wavelength (λ_1) can be calculated from the total seeing (r_{o,λ_2}) measured at another wavelength (λ_2) as follows:

$$r_{0,\lambda_2} = r_{0,\lambda_1} \times \left(\frac{\lambda_2}{\lambda_1}\right)^{6/5}. \tag{12}$$

TABLE 2. Statistical prediction of the seeing conditions at the Bohyun observatory

Conditions		Values								Unit
Spectral band		V	R	I	J	H	K	L	M	μm
Wavelength (λ)		0.55	0.64	0.88	1.22	1.65	2.20	3.55	4.77	
Fried parameter (r_o)	Worst (2σ)	6.6	7.9	11.6	17.2	24.7	34.8	61.9	88.2	cm
	Median	9.5	11.4	16.7	24.7	35.5	50.1	89.0	126.9	
	Best (2σ)	12.3	14.8	21.6	32.0	46.0	64.9	115.3	164.3	
Seeing (θ_{seeing})	Worst (2σ)	1.69	1.64	1.53	1.44	1.35	1.28	1.16	1.09	arcsec
	Median	1.17	1.14	1.07	1.00	0.94	0.89	0.81	0.76	
	Best (2σ)	0.90	0.88	0.82	0.77	0.73	0.69	0.62	0.59	
Critical time constant (τ_o)	Worst (2σ)	2.1	2.6	3.7	5.5	8.0	11.3	20.0	28.5	msec
	Median	3.6	4.3	6.3	9.4	13.4	19.0	33.7	48.1	
	Best (2σ)	5.7	6.9	10.0	14.9	21.4	30.2	53.5	76.3	
Greenwood frequency (f_G)	Worst (2σ)	63.3	52.8	36.0	24.3	16.9	12.0	6.8	4.7	Hz
	Median	37.5	31.3	21.3	14.4	10.0	7.1	4.0	2.8	
	Best (2σ)	23.6	19.7	13.4	9.1	6.3	4.5	2.5	1.8	
Isoplanatic angle (θ_0)	Worst (2σ)	0.86	1.03	1.50	2.23	3.20	4.51	8.02	11.43	arcsec
	Median	1.23	1.48	2.16	3.20	4.60	6.50	11.54	16.45	
	Best (2σ)	1.59	1.91	2.80	4.15	5.96	8.41	14.94	21.30	
Fundamental tracking frequency (f_T)	Worst (2σ)	1.03	0.89	0.64	0.46	0.34	0.26	0.16	0.12	Hz
	Median	0.65	0.56	0.41	0.29	0.22	0.16	0.10	0.07	
	Best (2σ)	0.43	0.37	0.27	0.19	0.14	0.11	0.07	0.05	
Isoplanatic tilt angle (θ_{TA})	Worst (2σ)	3.42	4.10	6.01	8.90	12.79	18.06	32.07	45.71	arcsec
	Median	4.92	5.91	8.66	12.81	18.40	25.99	46.16	65.79	
	Best (2σ)	6.38	7.65	11.21	16.59	23.83	33.65	59.76	85.18	

IV. AO SYSTEM DESIGN & PERFORMANCE ESTIMATION

4.1. AO System Design

The adaptive optics system is a laser-guide star (LGS) adaptive optics system for the 1.6 m telescope. The AO system consists of a tip/tilt secondary mirror, a deformable mirror, two scientific cameras (CCD and IR detector), a Shack-Hartman wavefront sensor, a sodium laser, and a data processing or control system. The adaptive optics system set is installed on an optical bench located on one of the Nasmyth ports, as shown in Fig. 5.

The incoming beam from the 1.6 m telescope is first beam-split into the guide camera and the main AO beam path. The guide camera is a wide field camera of 0.3° × 0.2° that serves as a finder-scope for aiming purposes. The main AO path beam is then re-collimated into a parallel beam of 24.5 mm diameter with recollimating optics, i.e. a parabolic mirror. The parabolic mirror also conjugates the exit pupil to the deformable mirror. The phase-corrected beam by the deformable mirror (DM) is then forwarded into a spectral beam splitter that reflects the whole beam but the V band centered at 589 nm, i.e. the sodium laser wavelength with 78.5 nm bandwidth for wavefront sensing (WFS). The visible and IR parts of the reflected beam are then reimaged on a low-noise electron-multiplying charge-coupled device (EMCCD) and a scientific instrument, respectively. Two scientific instruments are considered at this time, an IR imaging detector and an IR high resolution spectrograph.

Figure 6 shows three representative operation concepts (or modes) of the 1.6 m telescope with the adaptive optics system. First, the telescope can observe a bright target while wavefront sensing with it. Second, the telescope can

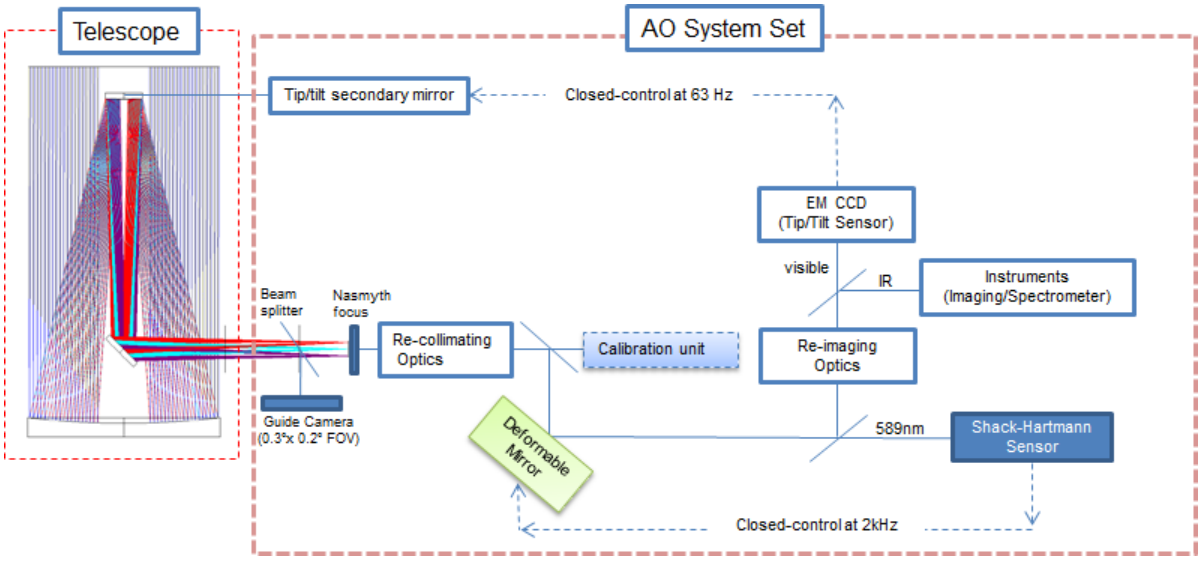

FIG. 5. Schematic diagram of the adaptive optics set.

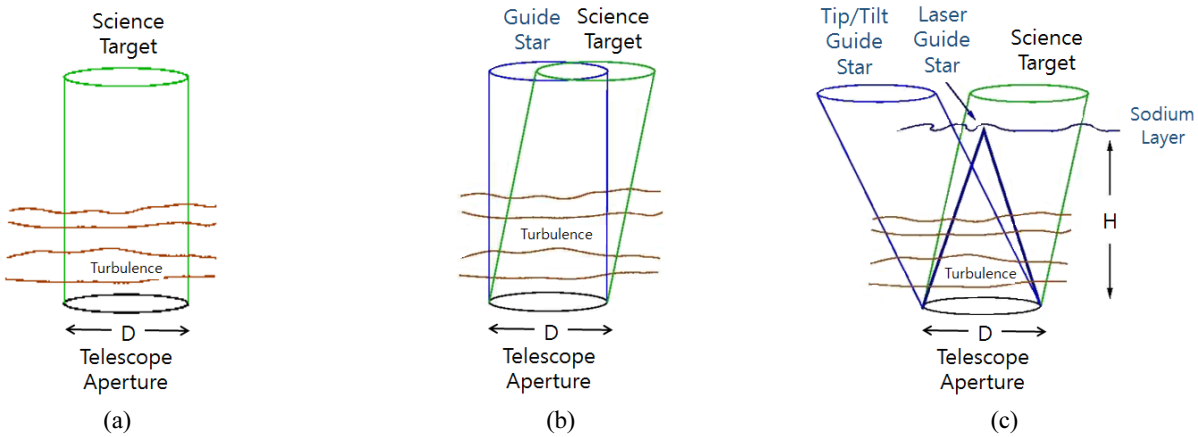

FIG. 6. Three representative operation concepts (or modes) of the 1.6 m telescope with the adaptive optics system. (a) Bright target observation with its own wavefront sensing (*None* mode), (b) Less bright target observation with NGS wavefront sensing (*NGS only* mode), (c) Faint target observation with NGS and tip/tilt LGS wavefront sensing (*LGS + NGS* mode).

observe a less bright target while wavefront sensing from a separate natural bright star called a natural guide star (NGS). Third, the telescope observes a faint target with wavefront sensing with a laser guide star. In this case, we need another bright natural star for tip/tilt sensing since the angular anisoplanatism blocks the tip/tilt sensing with the laser guide star. We name these three scenarios '*None*', '*NGS only*', and '*LGS + NGS*', respectively.

The system design of adaptive optics systems has been reported with the first order prediction of the system performance [1-9, 23-27]. Based on the first order prediction, we can find optimal values for the adjustable system-design parameters such as number of actuators, WFS sample rate, etc. Based on the seeing conditions in Table 2, the major optical components were optimally selected among commercially available components. Figure 7 shows pictures of the selected major AO components with their product numbers. Table 3 summarizes some key parameters of the components. It is worth mentioning here that beam reduction takes place during the conjugation from the telescope entrance pupil to the deformable mirror surface, as in Fig. 5. The Fried parameter of the seeing (r_0) is conjugated to the mirror with the beam reduction ratio (*BR*) as follows:

$$BR = (DM\ diameter)/(Telescope\ diameter), \tag{13}$$

$$r_{0,DM} = r_0 \times BR, \tag{14}$$

where $r_{0,DM}$ is the conjugated Fried parameter on the DM surface.

(a) (b) (c) (d)

FIG. 7. Pictures of the major components chosen for our adaptive optics system. The selected models are written in parentheses. (a) Deformable mirror (Alpao DM292 [28]), (b) Tip/Tilt secondary mirror mount (PI H824 [29]), (c) WFS sensor (AXIOM OCAM^{2}K [30]), (d) Tip/Tilt sensor (Nüvü Camēras HNü512 [31]).

TABLE 3. Principal parameters of the chosen AO components

Item	Parameters	Nominal value	Units	Comments
Deformable mirror	Pupil diameter (beam diameter)	24.5	mm	Alpao DM292 applied [28]
	Actuator pitch	1.5	mm	
	Array	16 × 16		
	Settling time	0.5	msec	
Wavefront sensing (Tip/Tilt)	Wavelength	broadband		Nüvü Camēras HNü512 EMCCD applied [31]
	Format	512 × 512		
	Frame rate	63	Hz	
	Quantum efficiency	>90	%	
	Dark noise	0.0002	$e^- pixel^{-1} frame^{-1}$	
	Readout noise	<0.1	$e^- pixel^{-1} frame^{-1}$	
Wavefront sensing (Shack-Hartmann sensor)	Wavelength	589	nm	Sodium laser
	Format	240 × 240		AXIOM Optics OCAM^{2}K with wavefront sensor option applied [30]
	Subaperture	20 × 20		
	Sampling frequency	2000	Hz	
	Quantum efficiency at 589 nm	90	%	
	Dark noise	0.01	$e^- pixel^{-1} frame^{-1}$	
	Readout Noise	0.1	$e^- pixel^{-1} frame^{-1}$	

4.2. Theory of AO System Performance Estimation

The first order performance estimation can be accomplished by several methods. The most frequently employed method is a statistical tolerance analysis method called the root squared sum (RSS) method. Here, σ_{SUM}^2 is the standard deviation of the entire system, σ_i^2 denotes the standard deviation of the i^{th} part, and n is the number of parts. In optics, σ_{SUM}^2 and σ_i^2 are the most commonly described terms of the root-mean-squared wavefront error (RMS WFE). Other important optical performance criteria, such as the Strehl ratio, can be predicted from the total RMS wavefront error as follows,

$$\sigma_{SUM}^2 \approx \sqrt{\sum_{i=1}^{n} \sigma_i^2}, \tag{15}$$

$$Strehl\ ratio = \exp\left(-\sigma_{SUM}^2\right). \tag{16}$$

In adaptive optics systems, the main error sources can be mostly divided into three groups: residual errors in telescope (σ_{TE}^2) instrumental factors in the adaptive optics system and external factors. The instrumental factors receive contributions from the components within an adaptive optics system. The instrumental errors include the wavefront fitting error of a deformable mirror (σ_{DM}^2), temporal errors due to pure time delays (σ_{TD}^2) and the limited bandwidth of the feedback loop (σ_{TR}^2), and measurement error of the wavefront sensor. The wavefront sensing error then consists of the aliasing error (σ_{AL}^2) and the noise error (σ_{DN}^2). The aliasing error is often called reconstruction error, which reflects the fact that the measurement device is only sensitive to low spatial frequency and the noise error is introduced by centroiding errors in the wavefront sensor, which is related to measurement of the signal-to-noise ratio. The external factors include the structure and dynamics of

TABLE 4. Major error sources of an adaptive optics system [1-9, 23-27, 32, 33]

Error Sources		Symbol	Equation in rad^2	Consideration		Note
				NGS	LGS	
Telescope	Telescope residual	σ_{TE}^2		Yes	Yes	Design residual + fabrication (uncorrectable) + dynamic
Instrumental	Fitting error of a DM	σ_{DM}^2	$0.28\left(\frac{d_s}{r_0}\right)^{5/3}$	Yes	Yes	Continuous thin-plate DM assumed d_s = actuator spacing on the entrance pupil
	Pure time delay	σ_{TD}^2	$28.4(\tau f_G)^{5/3}$	Yes	Yes	τ = time delay
	Limited bandwidth (Servo-lag)	σ_{TR}^2	$\left(\frac{f_G}{f_s}\right)^{5/3}$	Yes	Yes	f_s = system bandwidth
	WFS aliasing	σ_{AL}^2	$0.073\left(\frac{d_s}{r_0}\right)^{5/3}$	Yes	Yes	Can reduce down to $0.01(d_s/r_o)^{5/3}$ with the anti-aliasing Wiener filter [33]
	WFS detector noise	σ_{DN}^2	$\frac{\pi^2}{N_{ph}}\left(\frac{\theta_b d_s}{\lambda}\right)^2$	Yes	Yes	N_{ph} = No. of photons per integration time per sub-aperture $\theta_b = (\lambda/d_s)$ if $d_s < r_0$ and (λ/r_0) if $d_s > r_0$
External	Focal anisoplanatism	σ_{FA}^2	$\left(\frac{D}{d_o}\right)^{5/3}$	No	Yes	D = entrance pupil diameter $d_o = 0.046 \times H_{LGS} + 0.42$ [2]
	Angular anisoplanatism	σ_{AA}^2	$\left(\frac{\theta}{\theta_o}\right)^{5/3}$	Yes	Yes	θ = angular separation between a guide star and a scientific star
	Chromatism error	σ_{CR}^2	$\left(\frac{\alpha-1}{\alpha}\right)\left(1.03\left(\frac{D}{r_o}\right)^{5/3}\right)$	Yes	Yes	$\alpha = \frac{\Delta n(\lambda_1)}{\Delta n(\lambda_0)}$ with λ_1 and λ_0 are wavelengths of imaging and wavefront sensing, respectively
	Tilt measurement error	σ_{TM}^2	$\left(\frac{3\pi K_q \lambda_T}{16(SNR) r_0}\right)^2$	Yes	Yes	λ_T = wavelength of tip/tilt sensing, K_q = loss factor (1.3~1.5), SNR = signal-to-noise ratio
	Tilt temporal error	σ_{TT}^2	$\left(\frac{f_T}{f_{3dB}}\right)^2\left(\frac{\lambda_T}{D}\right)^2$	Yes	Yes	f_T = fundamental tracking frequency in eq. (7) $f_{=3dB}$ = system bandwidth, λ_T in μm and D in m.
	Tilt anisoplanatic error	σ_{TA}^2	$0.2\left(\frac{\lambda_T}{D}\right)^2\left(\frac{\theta}{\theta_{TA}}\right)^2$	Yes	Yes	θ_{TA} in eq. (9). λ_T in μm and D in m.

the atmosphere and the characteristics of the star or beacon used as the wavefront sensor. The external errors include the focal anisoplanatism (σ^2_{FA}) due to finite distance of a laser guide star, angular anisoplanatism (σ^2_{AA}) due to the angular separation between a guide star and an observation star, and chromatism error (σ^2_{CR}) due to atmospheric dispersion. Each term in the following equation can be estimated from the AO system and atmospheric parameters, as tabulated in Table 4.

$$\sigma^2_{SUM} = \sigma^2_{TE} + (\sigma^2_{DM} + \sigma^2_{TD} + \sigma^2_{TR} + \sigma^2_{AL} + \sigma^2_{DN}) + (\sigma^2_{FA} + \sigma^2_{AA} + \sigma^2_{CR} + \sigma^2_{TM} + \sigma^2_{TT} + \sigma^2_{TA}) \quad . \tag{17}$$

4.3. Performance Estimation

As tabulated in Table 5, we analyzed nine cases, three of each adaptive optics observation mode, as in Fig. 6. Each of the three cases applies stellar magnitudes of 5, 10, and 15 as the brightness of the observation target. In the case of the *NGS only* mode, the natural guide star (NGS) was assumed as 5 stellar magnitude and 1 arcsec angular separation. In the case of the *LGS + NGS* mode, all the guide stars were assumed as 5 stellar magnitude but with 1 and 4 arcsec angular separations, respectively.

Some errors mentioned in the above section depend on the number of photons arriving at the wavefront sensor. The total number (N) of photons arriving at the telescope in the visible region of the spectrum from a star of stellar magnitude m is given approximately by

$$N \approx 10^{4-m/2.5} \times A \times QE \times TR \times IT \times (\triangle\lambda), \tag{18}$$

where A is the area of the telescope in cm^2. *QE* is the quantum efficiency of the WFS and *TR* is the total transmission of the optics. *IT* is the integration time of each detector and $\triangle\lambda$ is the bandwidth in nm of the WFS. In this simulation, we assumed that the total optics transmittance is 50% and the WFS bandwidth ($\triangle\lambda$) is 80

TABLE 5. Nine analysis cases for the AO performance estimation

Simulation cases	1	2	3	4	5	6	7	8	9	Note
Operation mode	None			NGS only			LGS+NGS			
WFS guide star	None	None	None	NGS	NGS	NGS	LGS	LGS	LGS	
Tip/Tilt guide star	None	None	None	None	None	None	NGS	NGS	NGS	
Target stellar magnitude	5	10	15	5	10	15	5	10	15	
Guide star stellar magnitude	5	10	15	5	5	5	5	5	5	
Guide star angular separation	0.0	0.0	0.0	1.0	1.0	1.0	1.0	1.0	1.0	arcsec
Tip/Tilt guide stellar magnitude	5	10	15	5	10	15	5	5	5	
Tip/Tilt guide angular separation	0.0	0.0	0.0	0.0	0.0	0.0	4.0	4.0	4.0	arcsec

TABLE 6. AO performance estimation for the nine analysis cases

Simulation cases		1	2	3	4	5	6	7	8	9	Note
Error sources	Telescope residual (design)	79.1	79.1	79.1	79.1	79.1	79.1	79.1	79.1	79.1	nm
	DM fitting error	64.4	64.4	64.4	64.4	64.4	64.4	64.4	64.4	64.4	nm
	Pure time delay	26.1	26.1	26.1	26.1	26.1	26.1	26.1	26.1	26.1	nm
	Limited bandwidth	40.2	40.2	40.2	40.2	40.2	40.2	40.2	40.2	40.2	nm
	WFS aliasing	32.9	32.9	32.9	32.9	32.9	32.9	32.9	32.9	32.9	nm
	WFS detector noise	37.0	370.2	3701.5	37.0	37.0	37.0	37.0	37.0	37.0	nm
	LGS cone effect	0.0	0.0	0.0	0.0	0.0	0.0	55.5	55.5	55.5	nm
	Angular anisoplanatism	0.0	0.0	0.0	29.2	29.2	29.2	29.2	29.2	29.2	nm
	Tilt measurement error	0.0	0.0	0.0	0.0	0.0	0.0	0.0	0.0	0.0	nm
	Tilt temporal error	1.7	1.8	1.8	1.8	1.8	1.8	1.8	1.8	1.8	nm
	Tilt anisoplanatic error	0.0	0.0	0.0	0.0	0.0	0.0	22.9	22.9	17.2	nm
RSS expected	RMS WFE	123.1	388.3	3703.4	126.5	126.5	126.5	140.0	140.0	139.2	nm
		0.88	2.77	26.43	0.90	0.90	0.90	1.00	1.00	0.99	rad
	Strehl Ratio	0.42	0.06	0.00	0.41	0.41	0.41	0.37	0.37	0.37	

nm, which are common values in adaptive optics systems. In addition, the chromatism error (σ^2_{TM}) is due to the index fluctuations with respect to the wavelength. Since the correction given by the DM is proportional to the refractive index at the sensing wavelength, the residual wavefront for another wavelength is not null and is directly proportional to the input signal itself, with an attenuation coefficient depending on the index values of the two wavelengths. However, this proportionality is fully predictable and therefore we can reduce its effects in the following calculations and the effect is hence not considered.

Table 6 lists all the error terms and their expected WFE and Strehl ratio based on the RSS method. In this analysis, we commonly applied the worst (2σ) seeing conditions, as tabulated in Table 2. From the results, we can expect a Strehl ratio >0.3 in most seeing conditions with guide stars.

V. CONCLUSION

We presented a schematic layout of a 1.6 m telescope with a laser-guide star adaptive optics (AO) system. The AO system was designed based on the astronomical seeing conditions measured over a year at the Bohyun observatory, South Korea. Following an extensive investigation into the errors sources of the adaptive optics system with a sodium laser guide star, we concluded that we can achieve a Strehl ratio >0.3 over most of the seeing conditions with a NGS or the LGS guide star.

In this study, the laser guide star was assumed to be of 5 stellar magnitude based on previous experimental results from other astronomical observatories located at latitude similar to the Bohyun observatory. However, the intensity of the laser guide star depends on the density of sodium atoms at the mesosphere, which strongly varies locally and temporally. Further study is under preparation to predict the sodium density above the observatory and to predict the AO performance accordingly.

ACKNOWLEDGMENT

This research was supported by LigNex1 (Ltd).

REFERENCES

1. J. M. Beckers, "Adaptive optics for astronomy: principles, performance, and applications," Annu. Rev. Astron. Astrophys. **31**, 13-62 (1993).
2. R. K. Tyson, Principles of Adaptive Optics (CRC Press, Boca Raton, FL, USA, 2015).
3. S. S. Olivier, D. T. Gavel, H. W. Friedman, C. E. Max, J. R. An, K. Avicola, B. J. Bauman, J. M. Brase, E. W. Campbell, C. J. Carrano, J. B. Cooke, G. J. Freeze, E. L. Gates, V. K. Kanz, T. C. Kuklo, B. A. Macintosh, M. J. Newman, E. L. Pierce, K. E. Waltjen, and J. A. Watson, "Improved performance of the laser guide star adaptive optics system at Lick Observatory," Proc. SPIE **3762**, 2-7 (1999).
4. W. C. Rao, Y. Bo, C. Li, M. Li, X, Zhang, A. Zhang, C. Guan, L. Zhou, S. Chen, X. Hao, W. Ma, and Y. Zhang, "A sodium guide star adaptive optics system for the 1.8 meter telescope," Proc. SPIE **8447**, 84474K (2012).
5. C. d'Orgeville and G. J. Fetzer, "Four generations of sodium guide star lasers for adaptive optics in astronomy and space situational awareness," Proc. SPIE **9909**, 99090R (2016).
6. R. K. Tyson, "Adaptive optics system performance approximations for atmospheric turbulence correction," Opt. Eng. **29**, 1165-1173 (1990).
7. D. T. Gavel, J. R. Morris, and R. G. Vernon, "Systematic design and analysis of laser-guide-star adaptive-optics systems for large telescopes," J. Opt. Soc. Am. A **11**, 914-924 (1994).
8. B. W. Frazier, M. Smith, and R. K. Tyson, "Performance of a compact adaptive-optics system," Appl. Opt. **43**, 4281-4287 (2004).
9. M. A. van Dam, D. Le Mignant, and B. A. Macintosh, "Performance of the Keck Observatory adaptive-optics system," Appl. Opt. **43**, 5458-5467 (2004).
10. J. H. Lee, S. Shin, G. N. Park, H. Rhee, and H. Yang, "Atmospheric turbulence simulator for adaptive optics evaluation on an optical test bench," Curr. Opt. Photon. **1**, 107-112 (2017).
11. J. H. Lee, B. C. Bigelow, D. D. Walker, A. P. Doel, and R. G. Bingham, "Why adaptive secondaries?," Publ. Astron. Soc. Pacific **112**, 97-107 (2000).
12. E. Hecht, Optics (Addison Wesley, San Francisco, CA, USA 2002).
13. D. L. Fried, "Optical resolution through a randomly inhomogeneous medium for very long and very short exposures," J. Opt. Soc. Am. **56**, 1372-1379 (1966).
14. F. Roddier, "The effects of atmospheric turbulence in optical astronomy," Prog. Opt. **19**, 281-376 (1981).
15. F. Roddier, J. M. Gilli, and G. Lund, "On the origin of speckle boiling and its effects in stellar speckle interferometry," J. Opt. **13**, 263-271 (1982).
16. D. P. Greenwood, "Bandwidth specification for adaptive optics system," J. Opt. Soc. Am. **67**, 390-393 (1977).
17. G. Tyler, "Bandwidth considerations for tracking through turbulence," J. Opt. Soc. Am. **11**, 358-367 (1994).
18. R. R. Parenti, "Adaptive optics for astronomy," Lincoln Lab. J. **5**, 93-114 (1992).
19. J. H. Lee, S. J. Ro, K. Kim, T. Butterley, R. Wilson, Y. Choi, and S. Lee, "Robotic SLODAR development for seeing evaluations at the Bohyunsan Observatory," Advanced Maui Optical and Space Surveillance Technologies Conference (2015).
20. R. W. Wilson, "SLODAR: measuring optical turbulence altitude with a Shack-Hartmann wavefront sensor," Mon. Not. R. Astron. Soc. **337**, 103-108 (2002).
21. T. Butterley, R. W. Wilson, and M. Sarazin, "Determination of the profile of atmospheric optical turbulence strength from SLODAR data," Mon. Not. R. Astron. Soc. **369**, 835-845 (2006).
22. J. Vernin and F. Roddier, "Experimental determination of two-dimensional spatiotemporal power spectra of stellar

light scintillation Evidence for a multilayer structure of the air turbulence in the upper troposphere," J. Opt. Soc. Am. **63**, 270-273 (1973).
23. B. García-Lorenzo, A. Eff-Darwich, J. J. Fuensalida, and J. A. Castro-Almazán, "Estimation of adaptive optics parameters from wind speed: results for the Teide Observatory," Proc. SPIE **7476**, 74760F (2009).
24. B. García-Lorenzo, A. Eff-Darwich, J. J. Fuensalida, and J. A. Castro-Almazán, "Adaptive optics parameters connection to wind speed at the Teide Observatory: corrigendum," Mon. Notices Royal Astron. **414**, 801-809 (2011).
25. C. S. Gardner, B. M. Welsh, and L. A. Thopson, "Design and performance analysis of adaptive optical telescopes using laser guide stars," Proc. IEEE **78**, 1721-1743 (1990).
26. R. Flicker, "Efficient first-order performance estimation for high-order adaptive optics systems," Astron. Astrophys. **405**, 1177-1189 (2003).
27. J. W. Hardy, Adaptive optics for astronomical telescopes (Oxford University Press, New York, USA 1998).
28. https://www.alpao.com/adaptive-optics/deformable-mirrors.html (1 May. 2018).
29. https://www.physikinstrumente.com/en/products/parallel-kinematic-hexapods/hexapods-with-motor-screw-drives/h-824-6-axis-hexapod-700815/ (1 May. 2018).
30. http://www.axiomoptics.com/llc/ocam%C2%B2k/ (1 May. 2018).
31. http://www.nuvucameras.com/products/ (1 May. 2018).
32. M. S. Belen'kii, "Tilt angular correlation and tilt sensing techniques with a laser guide star," Proc. SPIE **2956**, 206-217 (1997).
33. C. M. Correia and J. Teixeira, "Anti-aliasing Wiener filtering for wave-front reconstruction in the spatial-frequency domain for high-order astronomical adaptive-optics systems," J. Opt. Soc. Am. A **31**, 2763-2774 (2014).